https://doi.org/10.5194/essd-2026-735
Preprint. Discussion started: 14 September 2026

Open Access Earth System Science Data Discussions

A global coastal tide model from multi-mission and wide-swath altimetry: GOAT-1C

Thomas C. Monahan[1*] and Michael G. Hart-Davis[2]

[1]Department of Engineering Science, University of Oxford, Thom Building, Parks Road, Oxford, OX1 3PJ, United Kingdom
[2]Deutsches Geodätisches Forschungsinstitut, Technische Universität München (DGFI-TUM), Munich, Germany
[*]Corresponding author(s): T. Monahan (thomas.monahan@eng.ox.ac.uk)

Abstract. A new global coastal tide model for non-polar regions is presented: GOAT-1C. The GOAT-1C atlas makes use of an admittance-based empirical tide estimation approach to infer residual coastal tidal variability omitted by the FES2022 tidal atlas from a combination of OpenADB nadir altimetry and, for the first time, wide-swath observations from the Surface Water and Ocean Topography mission. This approach builds on the Global Operator-based Admittance Tidal process framework (GOAT) which treats the global oceanic tidal response as a continuous function that can be learned using a DeepONet neural operator. The model shows improved performance in coastal regions in terms of variance reduction, tide gauges, and shoreline imagery relative to FES2022. Independent SWOT Cal/Val validation indicates that approximately 1% of coastal sea-level variance attributable to tidal-model error is associated with spatial structure resolved only at kilometre scales. Furthermore, using an ensemble approach, we provide per-constituent uncertainty estimates which allow users to understand where the product should be used and how much to trust it. Inclusion of wide-swath observations improves fine-scale corrections but must be handled with care. The final model and uncertainty estimates are released on a 4 km coastal grid.

1 Introduction

Coastal tides impact the lives of over 1 billion people and are essential to coastal biogeochemical processes (Brown et al., 2023). Despite their omnipresence, coastal tides remain one of the largest sources of uncertainty in global tide models due to a combination of complex variability, limited bathymetric quality and resolution, and historically poor altimetry data in these regions (Stammer et al., 2014). These model inaccuracies impact the wide range of downstream applications for which these models are used: from navigation (Turner et al., 2013), to flood modeling (Talke, 2025), to tide tables generated for beach-goers (Cartwright, 2000). In particular, as global sea-level rise continues, accurate tidal models in the coastal region will be increasingly important for nuisance flooding (Moftakhari et al., 2015).

Historical global tide modeling efforts have primarily focused on deep-ocean and shelf regions due to their importance as corrections for altimetry data (Stammer et al., 2014). However, with the launch of the Surface Water Ocean Topography mission (SWOT), accurate tidal corrections in coastal regions are of growing importance. Improvements in coastal tide models have come in three forms: (i) improved coastal bathymetry and parameterization tweaks, (ii) assimilation of coastal tide gauges, and (iii) advances in satellite altimetry processing (Hart-Davis et al., 2021).

https://doi.org/10.5194/essd-2026-735
Preprint. Discussion started: 14 September 2026

However, several advancements in coastal altimetry warrant the development of a new generation of empirical coastal tide models. First, new waveform retracking algorithms have greatly increased the reliability of historical altimetry data near the coast (Cazenave et al., 2022). In tandem, SWOT has provided an unprecedented view of coastal tides through wide-swath altimetry (Hart-Davis et al., 2024). Despite the potential of these data, challenges remain when combining them with classical nadir altimetry in typical tidal analyses. A combination of spatially and temporally correlated observations and errors presents unique challenges that must be addressed in the estimation process (Nilsson et al., 2026). Combined, however, these data sources dramatically increase the quantity and quality of data available for coastal altimetric tidal analyses.

In addition to new data, this work introduces a new framework for empirical altimetric tidal analyses, the Global Operator-based Admittance Tide model (GOAT), which exploits recent developments in both tidal analyses (Monahan et al., 2025a, b) and deep learning Lu et al. (2021). The approach encodes several physical features of the oceanic response into the model itself.

As the name suggests, GOAT-1C is restricted to the coasts where tides have the biggest societal impacts, in terms of compound flooding, navigation etc. Additionally, the coasts are where models tend to have the largest errors and the tidal variability becomes more spatially variable. While the proposed approach can be expanded globally, these reasons justify the focus on these regions in the present work. This manuscript briefly introduces the GOAT framework, the implementation used in the GOAT-1C atlas, and presents validation results using a range of independent metrics.

2 GOAT: Global Operator-based Admittance Tidal process model

GOAT is a general framework for learning time-invariant and spatially coherent response models of tidal processes, primarily from altimetry data. GOAT capitalizes on the fact that for tidal processes such as tides, storm surge, and tidal rivers, the ocean's response to forcing at a single location is both time-invariant and weakly nonlinear (Munk and Cartwright, 1966; Cartwright, 1968). This characteristic has served as the backbone of tidal analysis for centuries and is the basis of harmonic and response methods of tidal analysis. GOAT builds on these prior works and synthesizes several new ideas:

First, recent work has shown that this time-invariant relationship can also be established between hydrodynamic models and observational data (e.g. the errors these models make are systematic and can be represented by transfer functions) (Monahan et al., 2026). Unlike traditional empirical global tide models, which seek to model the residual between altimetry and a background model, GOAT explicitly learns a transfer function mapping the background model to the full sea level. In testing this was found to be advantageous, as the learned admittance function per location is simpler and can better exploit the prior provided by FES2022 (CNES, 2024).

GOAT also advances a new approach that treats the oceanic response as a continuous function in space. In this context, we argue the errors made by hydrodynamic models will be similar in neighboring locations. Typical empirical analysis procedures treat spatial locations as independent and thus do not exploit this feature explicitly (Hart-Davis et al., 2021). This presents major challenges in exploiting satellite altimetry data for modeling arbitrary tidal processes, as the altimetry observations of a single location can be many days apart.

https://doi.org/10.5194/essd-2026-735
Preprint. Discussion started: 14 September 2026

GOAT models the tide at a given location as a time-invariant mapping from lagged values of a base model $\hat{\zeta}$ to sea-level ζ. While one could also utilize gravitational forcing functions, as in the original response method (Munk and Cartwright, 1966), using an existing global model allows for simpler admittance functions to be inferred (Cartwright et al., 1969). For the sea-level ζ at a single location, we can construct a time-invariant operator $f(\hat{\zeta}) \rightarrow \zeta + \epsilon$, which relates the predicted sea-level $\hat{\zeta}$ from a base model, here FES2022 (CNES, 2024; Carrere et al., 2022), to some sea-level observations ζ and a residual ϵ. In this framing, f is a transfer function that takes as input time-lags of the predicted sea-level $\hat{\zeta}$, such that at a given location, $\hat{\zeta} = [\hat{\zeta}(t), \hat{\zeta}(t-\tau), \ldots, \hat{\zeta}(t-S\tau)]^T$. Here, $\tau = 2$ hours, and we include 12 lags (12 lagged values in addition to the real-time value). Justification for these values are provided in (Monahan et al., 2026)

We can generalize this approach to multiple locations by defining an operator $g(\hat{\zeta})(\theta, \lambda) \rightarrow \zeta(\theta, \lambda)$ that maps the modeled sea-level $\hat{\zeta}$ at geographical latitudes θ and longitudes λ to the associated sea-level $\zeta(\theta, \lambda)$ at the same point. Unlike f, which is defined as an operator in a single location, g, by construction, defines a continuous operator in space. Observe that in this framing, we do not require knowledge of the local bathymetry as is required by typical shallow water models. Instead, our approach exploits the fact that the nonlinear perturbations induced by flow over bathymetry can be learned directly from observational data.

We parameterize g using a DeepONet (Lu et al., 2021), which is a type of *neural operator*. Unlike typical neural networks, neural operators learn mappings between function spaces. An advantage of doing so is that the operator can both ingest and be queried at arbitrary locations. Both such features are crucial for exploiting altimetry data with its highly irregular sampling characteristics. In its most basic form, the DeepONet consists of two neural networks, typically referred to as the branch and trunk networks, trained in tandem. We represent the former using a Branch network $Branch(\hat{\zeta}) \rightarrow b$ which maps input functions $\hat{\zeta}$ to a latent representation $b = [b_0, b_1, \ldots, b_k]$ with $b_k \in \mathbb{R}$ for $k = 0, 1, \ldots, p$. The localized response is learned by a trunk network Trunk$(\theta, \lambda) \rightarrow d$ which takes in the location of the associated observation in Cartesian coordinates and produces a learned representation $d = [d_0, d_1, \ldots, d_k]$ with $d_k \in \mathbb{R}$ $k = 0, 1, \ldots, p$. The coordinates are mapped onto a unit sphere as a three-dimensional vector such that $x = \cos(\text{lat})\cos(\text{lon})$, $y = \cos(\text{lat})\sin(\text{lon})$, and $z = \sin(\text{lat})$. This formulation has the advantage of having no discontinuities. The networks are then combined through the dot product in a latent space such that

$$g(\hat{\zeta})(\theta, \lambda) = b_k \cdot d_k \approx \sum_{k=0}^{p} b_k \cdot d_k. \quad (1)$$

This produces a globally defined admittance which relates lags of the FES2022 predicted sea level to the altimetric data. Unlike a traditional finite impulse response filter, which can only shift energy between existing frequencies, the Branch network forms a nonlinear filter and can thus flexibly learn more complex frequency interactions. These were shown to be important, especially in shallow coastal regions Monahan et al. (2026). Several modifications are needed to apply this approach using both conventional and wide-swath altimetry. Details of the exact model configuration are provided in the GOAT-1C section below.

https://doi.org/10.5194/essd-2026-735
Preprint. Discussion started: 14 September 2026

3 Data

3.1 Along-track nadir altimetry

30 years of conventional satellite nadir altimetry were incorporated into this study, obtained from OpenADB (Schwatke et al., 2024), available at https://openadb.dgfi.tum.de/en/. A total of 31 altimetry datasets are used, namely from these missions: Sentinel-3A and -3B, Cryosat-2, Envisat, ERS1, ERS2, SWOT, Geosat, Jason 1-3, Sentinel-6A, Topex/Poseidon and Saral, including their respective geodetic and extended missions. All selected geophysical corrections remained consistent and were prioritised for coastal accuracy, particularly the use of the ALES retracker when available (Passaro et al., 2014). We follow a similar gridding strategy presented in (Hart-Davis et al., 2021), where we collect all sea level anomaly observations within a cap size that is a function of its latitude. By default, the sea level anomaly is corrected for the FES2022 tide model. However, this is added back so that the training objective is the total sea-level. Additionally, since we focus on the coastal zone, our data set only incorporates altimetry observations shallower than 500 meters. Finally, to account for land contamination of nadir altimetry, we only utilise data up to 3 km from the coast when the data is retracked by ALES, which is restricted to 10 km when using a different retracker. More information about the data used is available at https://openadb.dgfi.tum.de/en/products/sea-level-anomalies/.

3.2 SWOT KaRIn 2-km wide-swath altimetry

GOAT-1C incorporates observations from the SWOT Level-2 KaRIn Low Rate Sea Surface Height product (L2_LR_SSH, Expert group; version 2.0, `PGE_L2_LR_SSH` v5.4.0) SWOT project (2023). In contrast to conventional nadir altimetry, the Ka-band Radar Interferometer (KaRIn) provides two-dimensional measurements across swaths extending approximately 60 km to either side of the nadir track, separated by a central nadir gap. We use the geographically fixed, swath-aligned 2km grid. Training observations are drawn from the SWOT science orbit, which provides near-global coverage on a nominal 21-day repeat cycle; the independent validation set is drawn from the 1-day repeat calibration/ validation (Cal/Val) orbit, which repeatedly samples a fixed set of 28 ground tracks over a three-month period and is held out of training entirely.

For the science orbit we retain observations from cycles 1–53, spanning 2023-07-26 to 2026-07-18; for the Cal/Val orbit we retain cycles 474–578, spanning 2023-03-28 to 2023-07-11. The end-date of the Science orbit reflects the model development timeline. Future versions of GOAT-1C will be updated using more recent data. We apply the per-pixel quality information described in the L2_LR_SSH Product Description Document: we reject any pixel whose `ssha_karin_qual` flag sets a degraded or bad measurement, keep only open-ocean surfaces (`ancillary_surface_classification_flag` = 0), and discard $|\zeta| > 5$ m outliers. The learning target is constructed from the KaRIn sea-surface-height anomaly `ssha_karin` (with the alternate estimate `ssha_karin_2` used as a coastal fallback, where the primary field is edited to missing) plus the crossover correction `height_cor_xover`. All standard geophysical corrections are applied. As with the nadir altimetry, the ocean tide is added back to the SLA so that the model's training objective is the total sea-level rather than the tidal residual. We additionally exclude pixels lying more than 100 km from the coast, retaining only the coastal band relevant to the product. The resulting science-orbit dataset contains 1.11×10^9 valid KaRIn observations.

https://doi.org/10.5194/essd-2026-735
Preprint. Discussion started: 14 September 2026

3.3 Shoreline-Imagery Derived Constituents

We use tidal constituents derived from satellite-observed shoreline positions as an independent source of coastal validation. The dataset is based on the CoastSat multi-decadal shoreline archive for the Pacific Rim, which combines imagery from Landsat 5, 7, 8, and 9 over the period 1984–2026. It covers wave-dominated coastlines in Australia, New Zealand, Japan, Hawaii, California, Mexico, Peru, and Chile. CoastSat identifies the instantaneous water–sand interface in individual cloud-free images and intersects each detected waterline with shore-normal transects spaced at approximately 100 m intervals, producing irregularly sampled time series of cross-shore waterline position (Vos et al., 2019). In Hart-Davis et al. (2026), these data were used to derive tidal constituents using a harmonic analysis across the entire Pacific Rim. In this present study, we use the shoreline-derived M_2 constituent because it is the largest and most reliably resolved constituent under the sparse, sun-synchronous sampling of the Landsat missions. The resulting estimates provide validation directly at the land-ocean boundary, where conventional altimetry is least reliable, and are not assimilated into GOAT. They therefore offer a complementary test of whether improvements relative to existing tide models extend to the immediate coastal zone. The full derivation, quality control, and uncertainty characteristics of the shoreline constituent dataset are described by Hart-Davis et al. (2026).

4 Models

4.1 FES2022

GOAT learns a transfer function relating the tide predicted by an existing hydrodynamic model to the sea-level variability observed by satellite altimetry. We use the publicly distributed FES2022b ocean-tide solution as this prior model (Carrere et al., 2022). FES2022 is a global barotropic tide model constructed on an unstructured finite-element mesh. Its nominal mesh resolution varies from approximately 30 km in the open ocean to 10 km on continental shelves, 6 km near the continental slope, and 4 km in coastal regions, with additional regional refinements.

The FES2022 atlas contains 34 tidal constituents. Sixteen constituents are constrained through the assimilation of satellite altimetry and tide gauge estimates, while the remaining constituents are obtained from the corresponding hydrodynamic simulations. Although FES2022 is available on its native finite-element grid, it is also distributed on a regular ($1/30°$) grid, including an extrapolated coastal product intended to reduce missing predictions in estuaries and other poorly resolved coastal waters.

For every altimetric observation, we evaluate FES2022 at the observation location and time using PyTMD (Sutterley et al., 2025). The resulting tide predictions, including the lagged values defined above, are supplied to the branch component of GOAT. FES2022 is therefore used as a physically informed prior rather than as a correction that is simply added to the GOAT output. The learned operator is free to modify the amplitude, phase, and nonlinear structure of the prior response as a continuous function of location.

https://doi.org/10.5194/essd-2026-735
Preprint. Discussion started: 14 September 2026

4.2 GOAT-1C

GOAT-1C is trained on a combination of OpenADB nadir altimetry and SWOT Science Orbit data. The wide-swath observations provide unprecedented accuracy and resolution in complex coastal regions. However, they also present unique biases and imbalances when combined with the nadir data. Just considering raw data volume, the 2km KaRIn data from the Science Orbit contains approximately 19 times more observations. Despite this vast data volume, the data presents a different spatial and temporal bias on account of the observations concentrating around individual passes. The GOAT framework above represents the localized response with a single trunk that is continuous in space. The coastal response, however, varies over a wide range of length scales: a smooth, large-scale component that a low-dimensional continuous function captures well, and a fine-scale component that varies over a few kilometers. This component is concentrated around coastlines and sharp bathymetric gradients and is poorly approximated by a smooth global function. We therefore utilize a trunk with two heads.

A continuous head $\mathrm{Trunk}_c(\theta,\lambda) \to d^c$ retains the mesh-free coordinate network defined above, while a fine head attaches a free, node-specific latent vector $d_j^f \in \mathbb{R}^p$ to each node j of a dense ($\sim 4\,\mathrm{km}$) coastal grid. These codes are free parameters (not outputs of a coordinate network), regularized by weight decay and a graph-Laplacian smoothness penalty over the grid. Each observation is mapped to its nearest fine node, $j(\theta,\lambda) = \arg\min_j \|x(\theta,\lambda) - x_j\|$, and the trunk representation is the sum

$$d(\theta,\lambda) = d^c(\theta,\lambda) + \gamma_{j(\theta,\lambda)}\, d^f_{j(\theta,\lambda)}, \tag{2}$$

so the fine field is piecewise-constant in space: its coordinate dependence enters only through the discrete assignment $j(\theta,\lambda)$, giving the localized degrees of freedom that a smooth function cannot represent. The factor γ_j is a fixed coast-proximity gate, $\gamma_j = \sigma\big((D_0 - r_j)/s\big)$ with r_j the distance of node j to the coast, $D_0 = 15\,\mathrm{km}$ and $s = 5\,\mathrm{km}$, so the fine head is active near the coast and fades offshore; observations farther than 1.5 grid cells ($\approx 6\,\mathrm{km}$) from any fine node are routed to a null node and receive no fine contribution. As before, the sea level is recovered through the bilinear contraction given by Equation 1.

4.2.1 Training Objective

Because g ingests observations as (θ,λ,t,ζ) tuples and is agnostic to their sampling geometry, we assimilate conventional nadir altimetry and SWOT KaRIn swath altimetry within a single objective. For each SWOT sea-surface-height anomaly, we restore the crossover correction, apply standard quality editing, and treat every $\sim 2\,\mathrm{km}$ pixel as an independent observation, sampling the base model $\hat{\zeta}$ at the pixel's location and time to form its branch input exactly as for a nadir point. As SWOT resolves a dense two-dimensional swath, the observations constraining the fine head are overwhelmingly from SWOT pixels; conventional altimetry alone is too sparse along the coast to determine the dense grid.

Each altimeter pass carries an arbitrary DC offset, and the SWOT residual is further dominated by a mesoscale signal that no time-invariant response can explain. We accordingly train against an offset-invariant objective: within each pass (SWOT) or cycle (nadir) p, we remove the mean and a linear along-track trend of both the prediction and the observation before comparing them,

$$\mathcal{L} = \sum_p \left\| \mathcal{D}_p[\zeta] - \mathcal{D}_p[g(\hat{\zeta})] \right\|^2, \tag{3}$$

https://doi.org/10.5194/essd-2026-735
Preprint. Discussion started: 14 September 2026

where $\mathcal{D}_p$ denotes per-pass demeaning and detrending. The loss thus penalizes only the tidal variability the model is meant to learn and is invariant to the per-pass biases and long-wavelength drifts that carry none.

4.2.2 Uncertainty Estimates

The atlas also provides uncertainty estimates. However, it is important to be explicit about what this uncertainty represents. The uncertainty of the learned correction is estimated by retraining the model on 20 Poisson-resampled draws of the altimeter passes. For each node and constituent, this yields an ensemble of the complex correction $\Delta Z = Z^{\mathrm{GOAT}} - Z^{\mathrm{FES2022}}$, whose isotropic standard error is $\sigma = [\frac{1}{2}(\mathrm{Var}[\mathrm{Re}, \Delta Z] + \mathrm{Var}[\mathrm{Im}, \Delta Z])]^{1/2}$. Under the null hypothesis $\Delta Z = 0$ the statistic $|\Delta Z|^2/\sigma^2$ follows a χ^2 distribution with two degrees of freedom, giving a per-node p-value. Corrections are declared significant at a 5% false-discovery rate, controlled with the Benjamini-Hochberg procedure applied across all nodes separately for each constituent. This assumes the two components are bivariate-normal with negligible correlation and comparable variance. We validated the assumption against the full 2×2 ensemble covariance Σ by recomputing the Mahalanobis statistic $T_{\mathrm{full}} = \boldsymbol{\mu}^{\mathsf{T}} \Sigma^{-1} \boldsymbol{\mu}$ and re-running the identical FDR procedure. The Re/Im correlation is modest (median $|\rho| = 0.26$ over significant cells, consistent with 20-member sampling noise) and $T_{\mathrm{full}}/T_{\mathrm{iso}} = 1.000$ (5th–95th percentile 0.998–1.003). Only 0.03% of node–constituent classifications and 14 of $44{,}546$ nadir coastal nodes change. As such, the isotropic approximation is utilized.

Crucially, this uncertainty does not represent the total prediction error of the tide model. Rather, it quantifies the sensitivity of the learned GOAT correction to the finite and irregularly sampled altimetric training data, including the variability induced by resampling entire altimeter passes. It therefore measures how well constrained the inferred correction to FES2022 is by the available observations, rather than the uncertainty in the full tidal prediction. Errors that are common to GOAT and FES2022, unresolved physical variability, observational biases not captured by the bootstrap, and errors in the FES2022 prior itself are not necessarily represented. Accordingly, the resulting standard error should not be interpreted as a calibrated prediction interval for the total tide. This does not mean it has no utility; as will be shown using the metric defined in the subsequent paragraph.

4.2.3 Signal to noise ratio (SNR)

For each node and constituent, we summarise the reliability of the correction by its signal-to-noise ratio,

$$\mathrm{SNR} = \frac{|\Delta Z|}{\sigma} = \frac{\left| Z^{\mathrm{GOAT}} - Z^{\mathrm{FES2022}} \right|}{\left[\frac{1}{2}\left(\mathrm{Var}[\mathrm{Re}\,\Delta Z] + \mathrm{Var}[\mathrm{Im}\,\Delta Z]\right)\right]^{1/2}}, \tag{4}$$

i.e. the magnitude of the complex correction measured in units of its own ensemble standard error. The SNR is dimensionless and non-negative: it is the number of standard errors by which the correction departs from the null $\Delta Z = 0$, so an SNR of, say, 3 means the correction is three times larger than the uncertainty of the estimate. It is directly tied to the significance test above, since the χ^2_2 test statistic is exactly $|\Delta Z|^2/\sigma^2 = \mathrm{SNR}^2$; a correction with $\mathrm{SNR} \lesssim 1$ is indistinguishable from zero, whereas high-SNR corrections are those the model is most confident about. Unlike the amplitude $|\Delta Z|$, which only measures how large a correction is, the SNR measures how well *resolved* it is, and we use it as the primary confidence metric when stratifying skill by correction reliability.

https://doi.org/10.5194/essd-2026-735
Preprint. Discussion started: 14 September 2026

4.2.4 Atlas refinement

Testing showed that combining multiple tidal models yielded improved performance. At the subset of coastal nodes where the EOT20 atlas Hart-Davis et al. (2021) provides native (non-extrapolated) coverage, the GOAT correction is refined by a learned linear combination with a second, independently trained model whose branch ingests the EOT20 tide (the “EOT20-branch” DeepONet). Writing each model’s complex correction to FES2022 for constituent k as $\Delta Z_k^{\mathrm{G}} = Z_k^{\mathrm{GOAT(FES)}} - Z_k^{\mathrm{FES}}$ and $\Delta Z_k^{\mathrm{E}} = Z_k^{\mathrm{GOAT(EOT)}} - Z_k^{\mathrm{FES}}$, the blended correction is $\Delta Z_k^{\mathrm{blend}} = a_k \Delta Z_k^{\mathrm{G}} + b_k \Delta Z_k^{\mathrm{E}}$, where the per-constituent weights (a_k, b_k) are fit by least squares against the altimeter residual on a held-out validation fold and ridge-regularised toward the GOAT(FES2022) model ($a_k \to 1$, $b_k \to 0$) to prevent over-fitting. The blend is applied only to the 17 constituents that EOT20 resolves; the remaining constituents keep the GOAT correction, and the three non-tidal seasonal/radiational lines (S_a, S_{sa}, S_1) are excluded. Nodes carrying this refinement are flagged `eot20_blended`; at all other (“free”) nodes, the correction is the ensembled GOAT DeepONets alone, $Z = Z^{\mathrm{FES}} + \Delta Z^{\mathrm{G}}$. The reported uncertainty (SE, SNR, significance) is that of the GOAT DeepONet correction throughout; the EOT20 blend adds only a small but positive adjustment (median ~ 0.02 cm, reaching a few cm at macrotidal sites). We emphasize that the fold used to estimated the blend weights is distinct from the validation data used to produce the results below.

4.2.5 Atlas Description and Usage

The GOAT-1C atlas provides tidal constituents on a 4 km coastal grid spanning $\pm 66°$ latitude. Of the 34 constituents in FES2022, GOAT-1C estimates 31 and recommends 28 for general use (Table C2). After inspection, the S_1, S_a, and S_{sa} constituents were deemed unreliable in some regions so users should default to FES2022 for these three. A further three minor constituents present in FES2022 (λ_2, $MSqm$, MTm) are not resolved by GOAT-1C and should likewise be taken from FES2022. GOAT-1C supersedes FES2022 for the 28 recommended constituents and falls back to FES2022 for the remainder, so that a complete tidal prediction is always available. We also advocate including uncertainty estimates when using the atlas. Using the statistical significance procedure described above, users should only make use of the constituents when they are deemed significant. In cases where they are not, FES2022 should be employed (this is done throughout this manuscript). Depending on the objectives of the user, a more conservative threshold can be employed by making use of the location-specific SNR ratio defined above (also included in the final atlas). A complete description of the variables provided in the atlas and recommended usage is provided in Section C.

5 Assessment and Validation

To determine whether the improvements learned by GOAT generalize beyond its training observations, we assess the model using three complementary validation strategies. Withheld altimetry tests the effectiveness of the model as an operational tidal correction; Tide gauges test the accuracy of the recovered harmonic constants at fixed coastal locations; and shoreline-derived tidal estimates provide an additional independent assessment directly at the land-ocean boundary. We further consider these metrics in conjunction with the GOAT-1C uncertainty estimates. For all evaluations, *the corrections shown are the uncertainty-gated product; nodes failing the per-node joint-χ^2 significance test are muted (grey).* This follows from the recommended product usage described in Section C. Each validation metric is considered in detail in the following section. Together, these evaluations measure both constituent-level accuracy and the reduction of unresolved tidal variance in independent observations.

Here, "independent" primarily denotes independence from the observations used to train GOAT. Because FES2022 itself assimilates selected altimeter and tide gauge estimates, we separately identify or exclude validation records that overlap with the FES2022 assimilation dataset when sufficient metadata are available (pers. comms. Loren Carrere).

5.0.1 Validation data.

We explicitly restrict the data used in training in order to allow for fully out-of-sample validation. First, the nadir variance reduction is tested on a held-out 10% split ($2,420,947$ observations) of the multimission nadir-altimetry sea-level data (1993–2024, ≤ 800 observations per node). EOT20 blend coefficients are fit on a disjoint validation split of equal size. The remaining data are all used for training. For SWOT, all Cal/Val data are held-out and used for validation. An additional disjoint random 2% of the science-orbit pixels is reserved as a held-out science set on which the coast-binned variance reduction is reported. All other SWOT data are used for training. The random draws are made over individual observations, so validation and training share the same spatial and temporal support; full spatiotemporal independence is provided separately by the Cal/Val test window.

5.1 Variance Reduction

We evaluate each model through its ability to remove tidal variability from altimetric observations that were withheld from model training. This test is closely aligned with the principal application of a global tide model: providing an accurate geophysical correction for satellite altimetry. We estimate variance reductions from withheld OpenADB altimetry and both SWOT Cal/Val data and SWOT Science Orbit data.

Each candidate tide model is evaluated using the same observations, quality-control procedure, and set of non-tidal geophysical corrections. After subtracting the predicted tide, we calculate the variance of the residual sea-level observations at the associated location.

Performance is expressed both as an absolute residual variance and as the percentage variance reduction relative to FES2022,

$$\mathrm{VR}_m = 1 - \frac{\mathrm{Var}\,(r_m)}{\mathrm{Var}\,(r_{\mathrm{ref}})}, \tag{5}$$

where (r_m) is the residual obtained using model (m). Validation against FES2022 is done on identical data to ensure other non-tidal variability does not bias estimates.

https://doi.org/10.5194/essd-2026-735
Preprint. Discussion started: 14 September 2026

Open Access Earth System Science Data Discussions

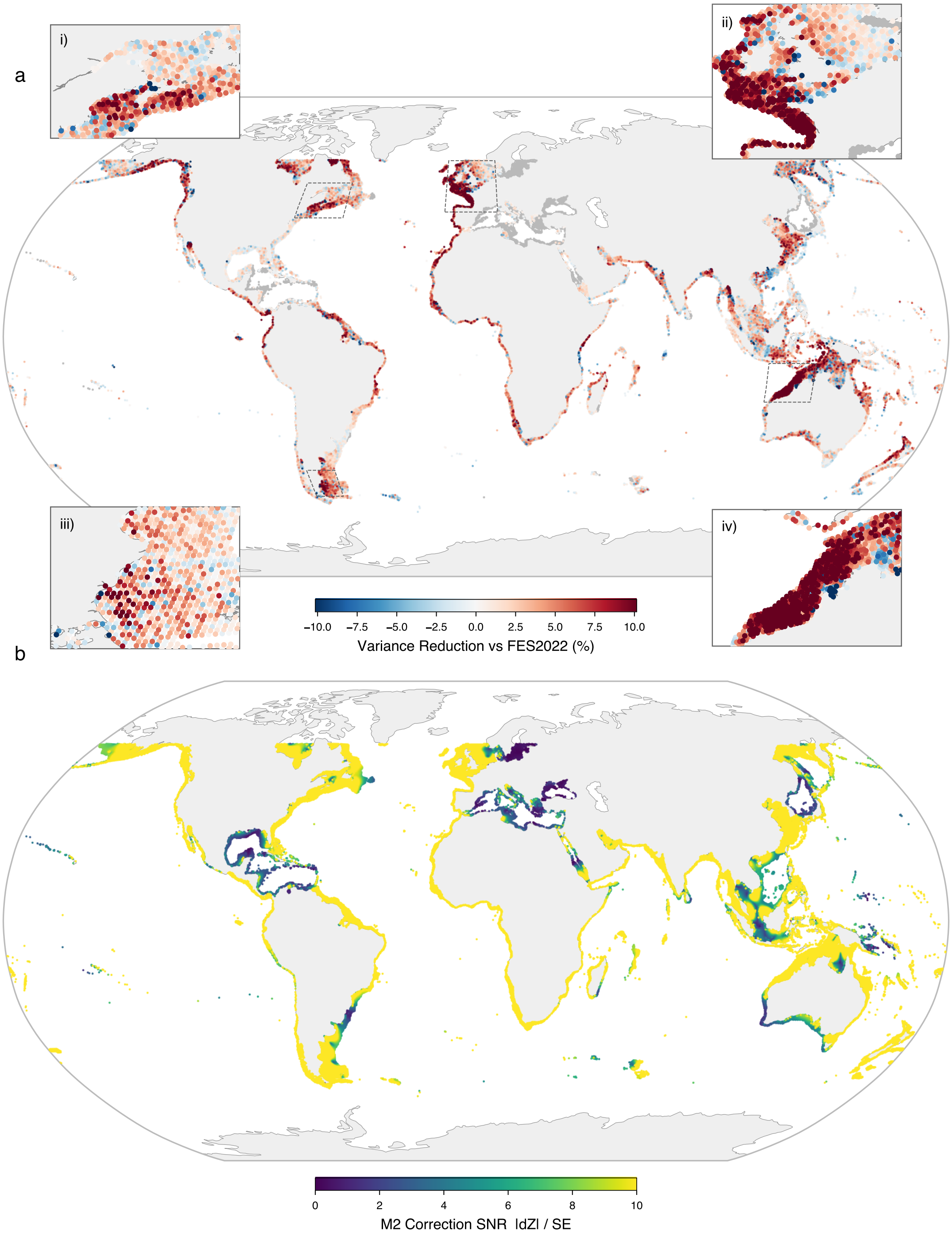

Figure 1. Variance reduction and correction confidence. a) Composite held-out-nadir variance reduction of GOAT vs FES2022. Inset panels are shown around areas with the largest corrections, corresponding to macro tidal regions in (i) Gulf of Maine, (ii) Northern European Shelf, (iii) Patagonian Shelf, (iv) North West Australia. Non-significant nodes are colored gray. b) Per-node signal-to-noise ratio of the M2 correction, |dZ|/SE, from the 20-member Poisson pass-bootstrap ensemble — yellow marks coasts where the learned correction is confidently non-zero. Both panels show only data within ±66° latitude.

https://doi.org/10.5194/essd-2026-735
Preprint. Discussion started: 14 September 2026

5.1.1 Total Variance Reduction

The learned correction reduces the held-out coastal altimetry-residual variance relative to FES2022 across the global coastal node set (Figure 1 Panel a). Pooled over all held-out observations, GOAT-1C achieves a net variance reduction of $+2.7\%$; because this pooled statistic is weighted by observation count and residual variance, it is dominated by the most energetic sites. For the 29,206 nodes where EOT20 was blended with the DeepONet solution, we obtain a pooled variance reduction of $+3.2\%$. For the global model (including both blended and un-blended nodes), the distribution of per-node variance reduction is correspondingly right-skewed, with a mean of $+2.4\%$ but a median of $+0.8\%$ ($n = 35{,}229$ nodes). This indicates that the typical coastal node improves by $\sim 0.8\%$ while a minority of high-energy macrotidal shelves account for the larger aggregate gain. The per-node bootstrap signal-to-noise ratio of the dominant M_2 correction (Figure 1 b) confirms that the correction is confidently non-zero along the majority of open coasts, and is largest and most robust through the macrotidal shelf seas shown in the insets.

Shelf regions carry the strongest improvements (Figure 1 Panel a), insets): the mean (median) per-node variance reduction is $+1.4\%$ ($+1.2\%$) across the Gulf of Maine (i), $+3.1\%$ ($+1.8\%$) in the Northern European shelf (ii), $+2.1\%$ ($+1.8\%$) on the Patagonian shelf, and $+6.6\%$ ($+6.0\%$) off northwest Australia. Unsurprisingly, these large variance improvements occur in macrotidal regions. In regions where FES2022 has assimilated gauges, particularly around the Northern European shelf, significant improvements are generally observed along the shelf break, with diminishing returns and even marginal degradation near gauges.

In contrast, microtidal regions are generally observed to be insignificant. This is reflected by grayed-out points in Figure 1 Panel a, and corroborated by the SNR estimates in Panel b. While the model does produce a correction at these locations, these values are not statistically trustworthy. Further discussion of uncertainty is provided in Section 5.4

5.1.2 Per-constituent Variance Reduction

Figure 2 attributes these variance reductions to individual constituents. Unsurprisingly, we find M_2 (+0.7%) and K_1 (+0.76%) yield the largest improvements in terms of total percentage variance reduction. The other major constituents S_2 ($+0.49\%$), with O_1 ($+0.28\%$) and P_1 ($+0.20\%$) also exceeding show more than 0.2% improvements. Several constituents are made slightly worse when considering global pooled variance reduction M_4, M_6, M_3, and M_M, all being less than 0.02%. These contributions mirror the model's own confidence: the constituents with the largest variance reduction are those the ensemble flags as highest signal-to-noise (Table A2). This is discussed further in the tide gauge validation section.

5.1.3 SWOT Variance Reduction

We also evaluate the performance of the model on a combination of SWOT Cal/Val data and held-out SWOT Science Orbit data. The former is fully independent, and the latter, whilst not observed in training, covers the same ground tracks. To evaluate the efficacy of the dual-headed coarse-and-fine model, we compare variance reduction on SWOT data when the model's resolution is artificially reduced. Figure 3 shows the SWOT variance reduction as a function of the distance to the nearest

https://doi.org/10.5194/essd-2026-735
Preprint. Discussion started: 14 September 2026

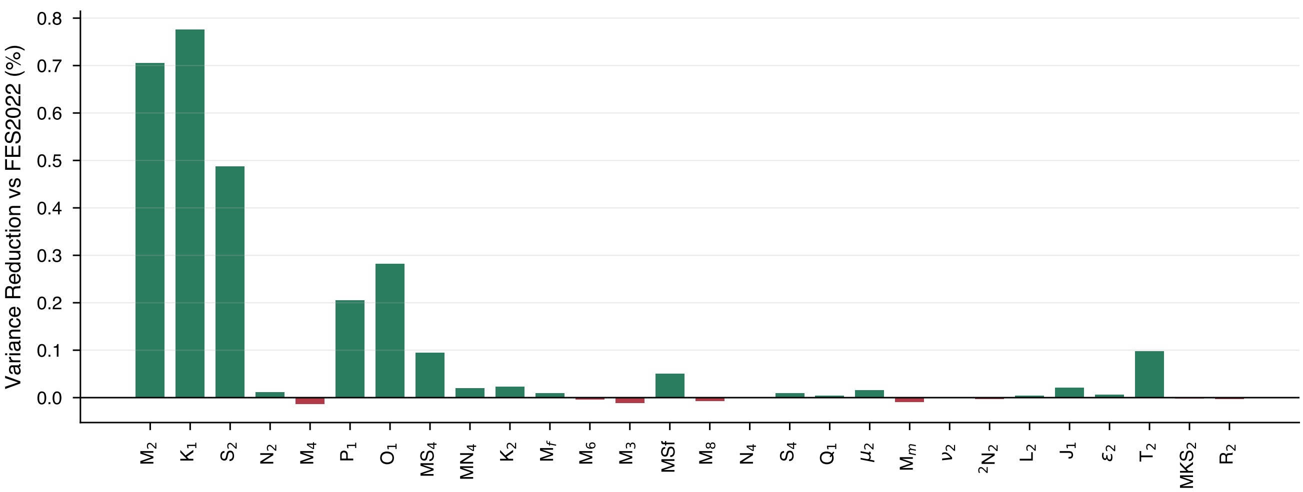

Figure 2. Per-constituent held-out-nadir variance reduction of GOAT vs. FES2022. Positive values (green) indicate GOAT reduces the altimetry-residual variance for that constituent; negative values (red) show GOAT increases altimetry-residual variance. Variance reduction is computed relative to the total SLA at a given location. The product reverts to FES2022 where a correction is not statistically significant. Significance is assigned where the complex correction $\Delta Z = Z^{\mathrm{GOAT}} - Z^{\mathrm{FES2022}}$ differs from zero at a 5% Benjamini–Hochberg false-discovery rate, using the χ^2_2 statistic $|\Delta Z|^2/\sigma^2$ with σ^2 the variance of ΔZ over a 20-member pass-bootstrap ensemble.

node (effective model resolution) for both orbits. We compare the coarse head only, whose resolution is approximately 25 km, with the dual-headed model (i.e. including the fine head). We observe that the models native resolution, given by the 0-2 km distance to the nearest fine node, yields a $\approx 1.2\%$ variance reduction relative to FES2022 across both orbits. The Cal/Val result (Panel a) provides independent validation that the small-scale performance improvements are real. Decreasing the resolution (or increasing distance from node to SWOT observation) decreases the benefit of the model, eventually saturating at the coarse-only floor. This appears to be more gradual on the Cal/Val data than the Science orbit. However, this may just be a consequence of the sampling of the test data. This result illustrates that the dual-head model improves the resolution of fine-scale tidal variability relative to FES2022; however, this improvement only exists if the model is used at high resolution. Given the growing importance of this fine-scale variability, models will increasingly be limited by their resolution (and observation resolution), requiring improvements in these areas to be prioritized for complicated coastal geometries. Future global model development, particularly for application to SWOT, will therefore need to achieve such resolutions, as we have started to do here.

5.2 Gauge Validation

Tide gauges provide the most direct validation of the recovered harmonic constants at fixed coastal locations. We compare GOAT-1C and FES2022 against constituent estimates from TICON4 Hart-Davis et al. (2025). To reduce dependence between

https://doi.org/10.5194/essd-2026-735
Preprint. Discussion started: 14 September 2026

Open Access Earth System Science Data Discussions

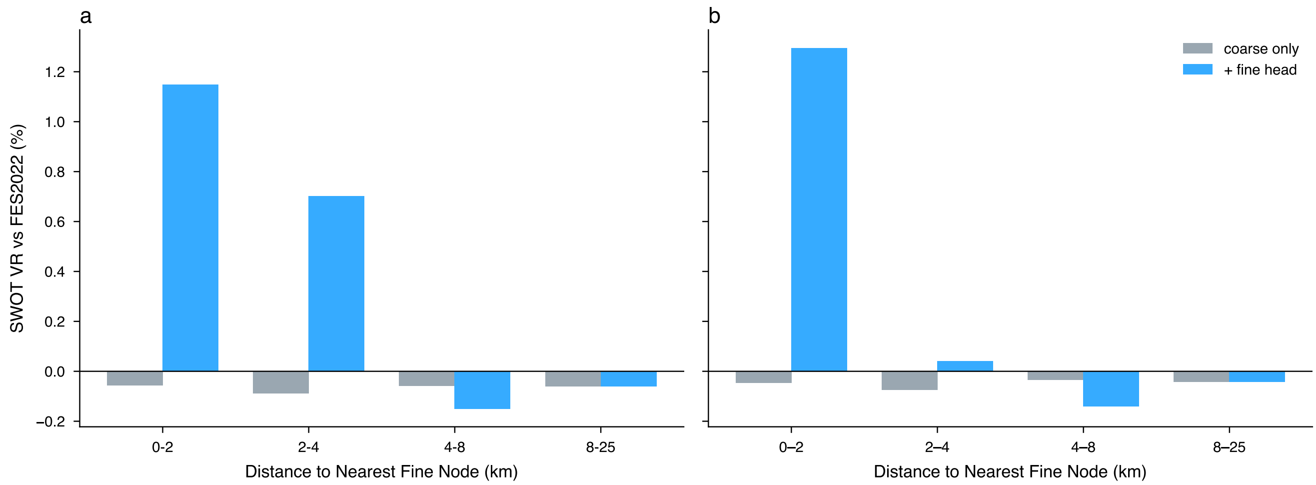

Figure 3. GOAT-1C variance reduction versus FES2022 on held-out SWOT observations using both (a) Cal/Val and (b) Science orbit data. Computed by predicting the GOAT-1C tide at each SWOT-KaRIn pixel's exact location and time with the dense 4 km fine head (light blue) and without it (grey, coarse trunk only ≈25 km resolution), binned by distance to the nearest fine node. Variance reductions estimated from 2,000,000 points from each orbit. Note: fine-head skill at 0-2 km reflects the expected performance of the released GOAT-1C atlas. The Cal/Val orbit is completely independent. While Science orbit data were held out, the model was trained on observations from the same tracks. Both panels share a y-axis.

the validation dataset and the FES2022 prior, gauges known to have been assimilated into FES2022 are excluded (pers. comms. Loren Carree). Model estimates are sampled at the nearest GOAT-1C coastal node, subject to a maximum gauge-to-model separation of 15 km. After this filtering, a total of 514 gauges remain for validation.

For each tidal constituent k, model performance is quantified using the complex harmonic-vector error,

$$E_k = \left|Z_k^{\text{model}} - Z_k^{\text{gauge}}\right| = \left|A_k^{\text{model}} e^{i\phi_k^{\text{model}}} - A_k^{\text{gauge}} e^{i\phi_k^{\text{gauge}}}\right|, \tag{6}$$

where A_k and ϕ_k denote the constituent amplitude and phase lag under a common convention. We additionally report amplitude and phase errors separately. This vector-error metric jointly accounts for errors in constituent amplitude and phase and is therefore used as the primary gauge-validation metric.

A key feature of GOAT-1C is that each learned complex correction,

$$\Delta Z_k = Z_k^{\text{GOAT}} - Z_k^{\text{FES2022}}, \tag{7}$$

is accompanied by an uncertainty estimate derived from the 20-member Poisson pass-bootstrap ensemble. We define the correction signal-to-noise ratio as

$$\text{SNR}_k = \frac{|\Delta Z_k|}{\text{SE}(\Delta Z_k)}, \tag{8}$$

https://doi.org/10.5194/essd-2026-735
Preprint. Discussion started: 14 September 2026

where $\mathrm{SE}(\Delta Z_k)$ is the ensemble-derived standard error of the complex correction. Statistical significance is assessed from the bootstrap ensemble and corrected for multiple testing using the Benjamini–Hochberg false-discovery-rate procedure. Unless otherwise stated, the uncertainty-gated GOAT-1C product applies the learned correction only where it is statistically significant and otherwise reverts to the FES2022 prior.

Table 1 summarizes the gauge benchmark for constituents whose GOAT corrections are sufficiently well constrained globally, while results for all available constituents are provided in Table A1. Across the constituents shown in Table 1, GOAT-1C produces small but broadly consistent improvements over FES2022. The mean complex RMS error decreases from 4.67 cm to 4.63 cm and the median complex error from 0.74 cm to 0.72 cm. The largest RMS reductions are found for K_1, O_1, MS_4, and MN_4, while several smaller constituents remain close to parity with FES2022.

These improvements are modest when aggregated globally, which is consistent with the role of FES2022 as a high-quality prior already constrained by both altimetry and tide gauge observations. GOAT-1C, therefore, is not reconstructing the tidal field independently but instead learning spatially coherent residual corrections to an already accurate global solution. In addition, the gauge benchmark assigns approximately equal weight to a sparse set of fixed coastal locations, whereas the largest GOAT-1C improvements occur in geographically localized energetic shelf and macrotidal regions (Figure 1). The small global-average gauge improvement is therefore compatible with the much larger regional variance reductions observed in those areas.

To determine whether the aggregate improvements are driven by a small number of gauges or instead reflect a systematic shift in performance, we additionally evaluate the paired change in complex error,

$$\Delta E_k = E_k^{\mathrm{FES2022}} - E_k^{\mathrm{GOAT}}, \tag{9}$$

such that $\Delta E_k > 0$ indicates an improvement relative to FES2022. In contrast to RMS error, this metric reflects the error at a single location in sea-level units (here, cm). In tandem, we assess whether the ensemble-derived confidence metrics are predictive of realized model skill. Figure A1 evaluates the M_2 improvements as a function of the Correction SNR using both independent TICON gauges and the held-out nadir data. Across both datasets, we observe an increase in model skill with Correction SNR, reflected by a Spearman $\rho = +0.28$ for both. The relationship between realized skill and correction SNR was found to be largely robust across constituents (these are reported in Table A2). These results provide independent evidence that the SNR is a useful indicator of where the learned GOAT correction is most likely to improve upon FES2022.

5.3 Shoreline Validation

Recent work has demonstrated that tidal constituents can be estimated from time series of satellite-derived shoreline positions (Hart-Davis et al., 2026). Here, the shoreline position can be related to the associated water level with prior knowledge of the beach slope through a simple trigonometric transformation. While, these data are imperfect, they provide a complementary validation source because they sample the immediate coastal boundary, where conventional altimetry frequently becomes sparse or less reliable, and they are not used to train GOAT-1C or used in the construction of FES2022 or any other existing models. Due to the sun-synchronous nature of these satellites, we here restrict our comparison to the principal lunar semi-

Table 1. TICON4 benchmark with GOAT correction applied only where significant (e.g. nodes passing the constituent-specific 5% FDR significance test described in 4.2.2). Bold values indicate a model is better on a given metric. Gauges are used if they are within 15 km of a model node and not assimilated into FES2022 (n = 514). Constituents are included only if they are significant at ≥ 10% of gauges. Full constituent results, including those deemed insignificant, are provided in Table A1.

	RMS (cm)		Median (cm)		Amplitude error (cm)		Phase lag error (deg)	
Constituent	FES2022	GOAT	FES2022	GOAT	FES2022	GOAT	FES2022	GOAT
M_2	21.41	**21.32**	2.71	**2.54**	**1.23**	1.25	3.4	**3.2**
S_2	**5.56**	5.57	**1.13**	1.13	**0.50**	0.58	4.9	**4.7**
N_2	4.34	**4.33**	0.70	**0.70**	**0.33**	0.33	4.3	**4.1**
K_2	**1.73**	1.73	0.45	**0.45**	**0.21**	0.21	6.1	**6.1**
K_1	5.77	**5.63**	0.83	**0.82**	0.39	**0.37**	**3.2**	3.5
O_1	3.91	**3.87**	0.70	**0.65**	0.37	**0.36**	3.0	**2.8**
P_1	1.51	**1.50**	0.38	**0.38**	0.23	**0.23**	**4.6**	4.6
Q_1	**0.86**	0.86	**0.23**	0.23	**0.12**	0.12	4.6	**4.6**
M_4	2.87	**2.84**	**0.44**	0.46	**0.23**	0.23	**25.7**	26.0
MS_4	2.25	**2.17**	0.29	**0.28**	0.14	**0.14**	45.5	**43.7**
MN_4	1.19	**1.15**	**0.24**	0.24	0.11	**0.11**	47.5	**46.5**
Mean	4.67	**4.63**	0.74	**0.72**	**0.35**	0.36	13.9	**13.6**

diurnal constituent M_2. As the derivation of tides from shorelines matures through improved processing, additional constituents can be included in future comparisons.

We compare each model's M_2 constituent with shoreline-derived estimates across Pacific coastlines in Figure 4. At each beach-transect, the models are evaluated at the location associated with the shoreline estimate, and performance is quantified using amplitude, phase, and total RMS error. It can be seen that while site-to-site results are mixed, 65% of sites improve overall, albeit marginally (order mm). While this suggests GOAT-1C is having a small positive change at the coast, nominal changes are dominated by the noise of the shoreline estimates themselves. Validation in (Hart-Davis et al., 2026) showed 5.77 cm and 4.07 degree errors with TICON4 gauges. Since none of the shoreline estimates overlap with the macrotidal regions which showed large variance reductions in Figure 1, this is to be expected. Future work to extend the shoreline-derived tidal atlas to macrotidal coastlines is thus warranted to enable future global model validation with these data.

5.4 Uncertainty

A key feature of the GOAT-1C atlas is the estimation of uncertainty at a per-constituent level. The global distribution of uncertainties per-constituent is itself informative about both where the productshould be used, and where future model development is warranted in existing global tide models. Figure 5 shows the estimated SNR and significance of each constituent at all 44,546

https://doi.org/10.5194/essd-2026-735
Preprint. Discussion started: 14 September 2026

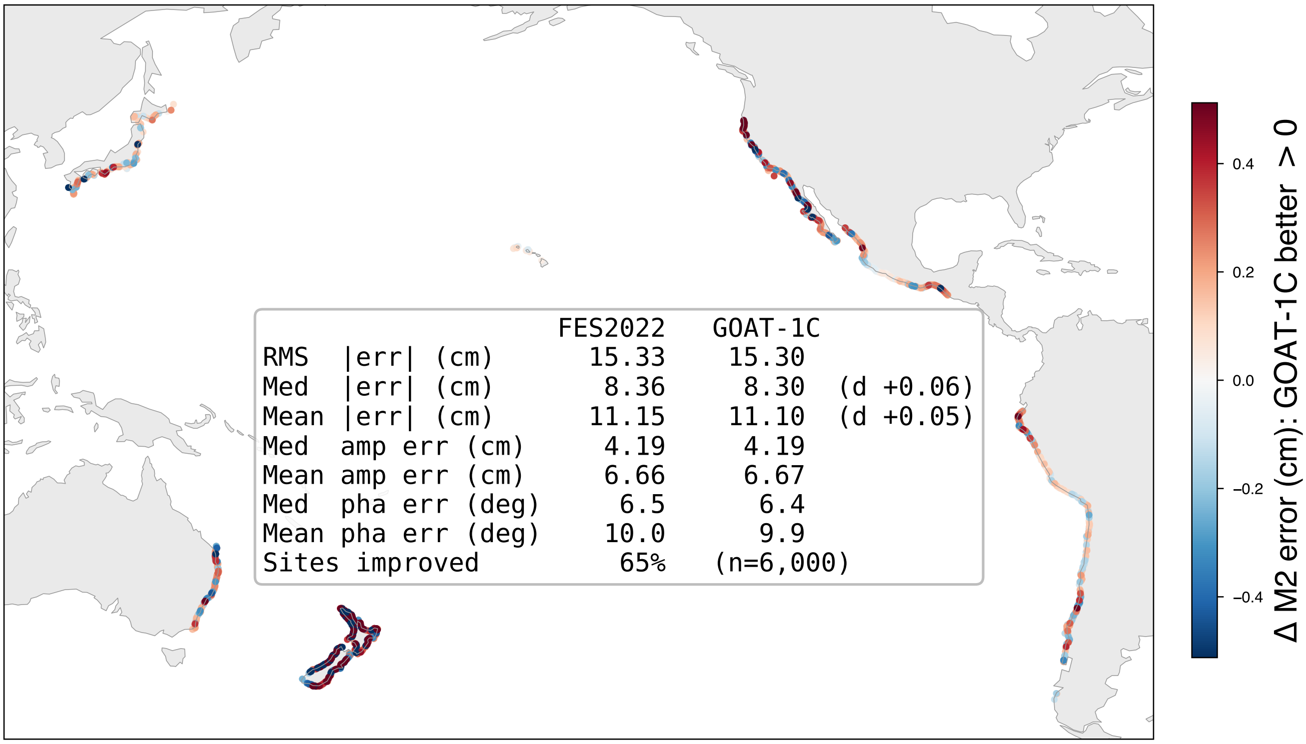

Figure 4. Shoreline-imagery estimated M2 error, GOAT-1C versus FES2022. Each Pacific shoreline site ($n = 6{,}000$) is coloured by $\Delta = |\mathrm{err}|_{\mathrm{FES2022}} - |\mathrm{err}|_{\mathrm{GOAT-1C}}$, the difference in complex M2 vector error against the independent shoreline harmonic M2 estimates: red = the GOAT-1C prediction is closer to the shoreline M2 than FES2022, blue = FES2022 is closer. Statistics are reported for both vector errors and amplitude and phase.

nadir altimetry nodes. It can be seen that no constituent is significant everywhere, with M_2 unsurprisingly being the most globally present, with 91% of nodes being significant. K_1 yielded the largest global variance reduction and is significant at 81% of locations. In contrast, it can be seen that the derived long-period constituents Mf, Mm and MSf have low global significance of 14%, 5% and 18%, respectively. Correlating the per-constituent percentage variance reduction with the global significance percentage yields a Pearson correlation of $r = 0.82$, indicating that more significant constituents generally yield greater variance reduction. However, a node being significant does not necessarily mean the correction is large; rather, it indicates that the node is trustworthy.

We stress that the ensemble spread quantifies uncertainty in the learned correction rather than uncertainty in the total predicted tide. This is a direct consequence of how the estimate is produced by ensembling models. Consistent with this interpretation, the raw correction standard error was not found to predict lower absolute out-of-sample gauge error. However, the magnitude partly covaries with the magnitude of the correction itself. We therefore do not interpret the ensemble standard

https://doi.org/10.5194/essd-2026-735
Preprint. Discussion started: 14 September 2026

Open Access Earth System Science Data Discussions

error as a calibrated prediction interval for GOAT-1C sea level and make no nominal gauge-error coverage claim. Instead, the objective of the provided uncertainties and correction SNR values is to provide a useful empirical confidence measure which indicates where and where not to use the model. This has been corroborated with independent gauge and held-out altimetry skill increasing with SNR in Figure A1 and Table A2.

6 Discussion

To the best of our knowledge, GOAT-1C is the first global tide model to make use of SWOT wide-swath observations. As shown, combining these data with retracked nadir altimetry improves coastal tide estimation across a range of validation metrics. These gains are a consequence of both the improved data available and the methodological innovations presented.

Our testing (not shown) found that training a model jointly (e.g. not separating into two heads) on SWOT and nadir altimetry yielded sub-optimal results when tested on held-out data from both platforms. This is a combination of a number of effects. The SWOT data contain unique sources of errors, roll errors, and submesoscale variability unresolved in conventional altimeters. In addition, the errors cannot be assumed to be independent as they are simultaneously spatially dense and temporally sparse. These errors must be dealt with in the corresponding regression in order to yield satisfactory results. The approaches adopted to mitigate these errors largely follow from recent work on the mean sea surface by (Nilsson et al., 2026). It is to be expected that as the orbit of SWOT continues and processing continues to improve, the accuracy of model predictions will also improve.

Our methodology brings together several key innovations inspired by the long history of the tidal response method. First, we show that residual tidal variability from altimetry can be captured effectively using an admittance-based approach, which relates the total modelled tide to observational data. This follows from some of the earliest work with Munk and Cartwright's response method, which found this to yield simpler admittances that can be easier to infer (Zetler and Munk, 1975; Cartwright et al., 1969). Just as with a harmonic approach, an advantage of these response-based approaches is the fact that they require no knowledge of the local bathymetry. As such, they may be especially useful around unsurveyed coastlines whose high bathymetric uncertainties limit the efficacy of hydrodynamic models.

Second, we advance a spatially coherent approach which enforces that these admittances smoothly vary in space. This too follows from the suggestion of Cartwright and Ray (Cartwright and Ray, 1990). However, this work shows that the spatially coherent approach can be applied using a background tide model rather than the equilibrium potential. The assumption of spatial coherence naturally regularises the model solutions and reduces overfitting to the submesoscale signal and other altimetry noise. In addition to regularisation, spatial coherence also enables the model to make use of information from neighbouring locations. This approach may have value in extracting *more* information about solar and diurnal tides from sun-synchronous missions by capitalizing on the fact that the length-scale of tides is generally larger than the separation between ground-tracks. The derived solar and diurnal constituents are only as good as this assumption. Hence, we emphasize that while this may minimize the negative impacts of sun-synchronous missions, non-sun-synchronous sampling is essential for tidal research.

This work is the first to include shoreline imagery-derived tides in the validation of a global tide model. These data constitute an independent data source of data which has not been assimilated into any global solutions, nor empirically ingested. The

https://doi.org/10.5194/essd-2026-735
Preprint. Discussion started: 14 September 2026

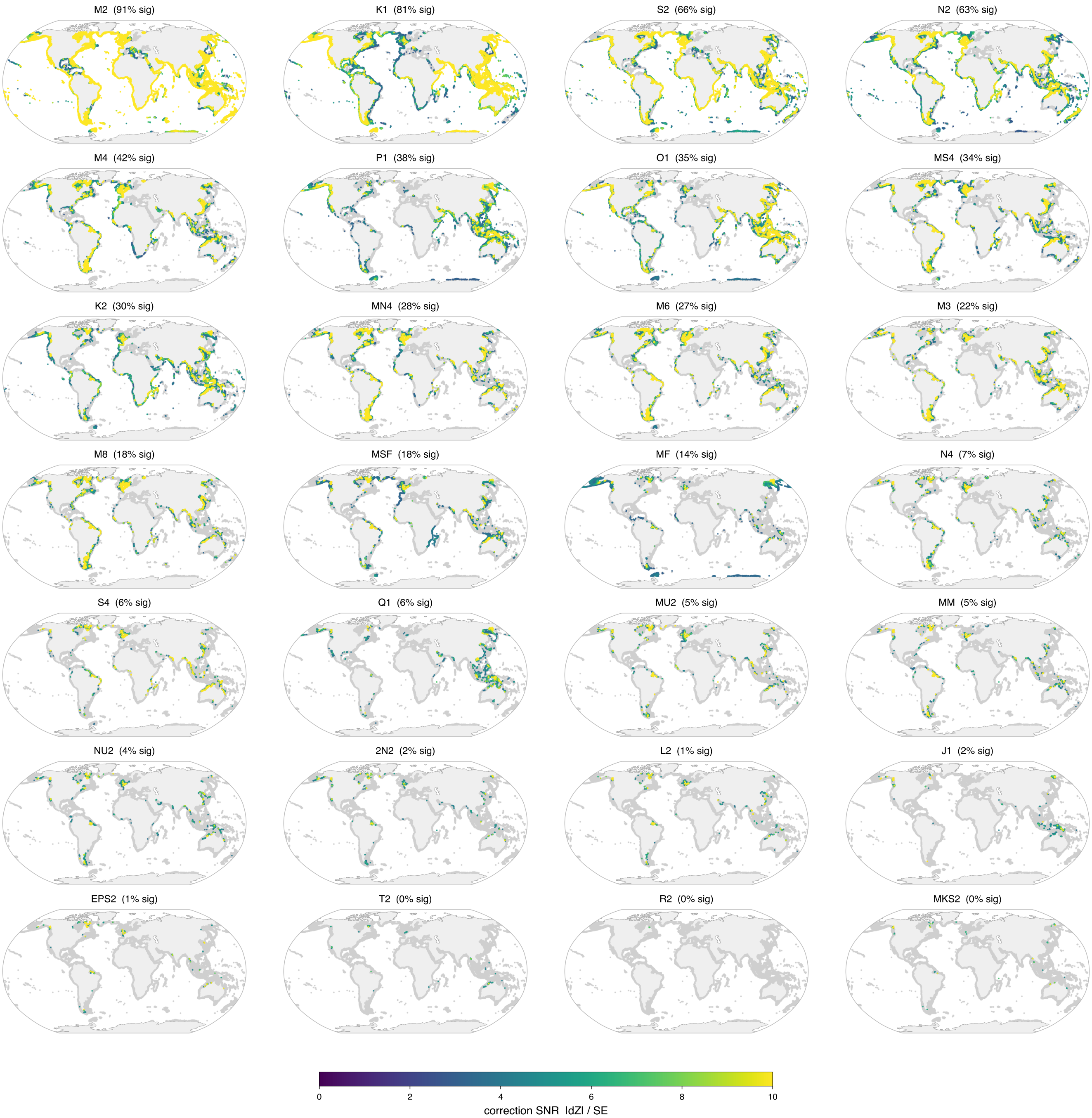

Figure 5. Per-constituent correction SNR maps. For each tidal constituent, the global coastal-node field of the learned correction's bootstrap signal-to-noise ratio (|dZ|/SE), with nodes that do not pass that constituent's Benjamini–Hochberg FDR test greyed out. Panel titles give the fraction of nodes significant for each constituent.

https://doi.org/10.5194/essd-2026-735
Preprint. Discussion started: 14 September 2026

findings from our validation of these data, compared with the other metrics employed, suggest that they are valuable for providing insights into model performance on the coast. Their long record of observations and fine-scale resolution, these data provide an additional valuable resource for coastal research that could motivate the inclusion of these data into future models, especially within the GOAT framework. Validation with these data also demonstrated that the present shoreline atlas, restricted to the Pacific basin, is limited in its coverage of macrotidal regions. Future global expansion of the shoreline inferred tides should therefore be prioritized in order to improve the utility of these data for global model validation. This should include extensions to different geographical regions, and an expansion of the satellite imagery platforms, potentially making use of private imaging satellites.

As discussed throughout the text, the empirical GOAT-1C atlas may be useful in informing future model development efforts. It remains to be said how this can be done. First, it is worth clarifying that the success of the proposed approach is a direct consequence of the already excellent FES2022 atlas. This quality is reflected by the fact that in many regions the altimetry-derived model is near parity with FES2022. However, as shown, there are also a number of complex coastal regions where this is not the case. Regardless, the approach exploits the high-quality prior solution FES2022 provides in order to estimate simpler admittance functions which transfer this solution to that observed from altimetry. The resulting atlas could therefore be viewed as an observationally constrained discrepency estimate of the FES2022 atlas in coastal regions. We illustrate this in Appendix Figure A2. These post-hoc altimetry-derived FES2022 uncertainty estimates are also released with the GOAT-1C atlas. Future model improvement efforts, particularly boosts in resolution and bathymetric tweaks, should focus on regions with the greatest "uncertainty" (e.g. those characterized by the largest GOAT variance reductions). Northwest Australia and the shelf-break of the Northern European Shelf appear to be prime candidates. The SWOT variance reduction results show that the fine-head can remove an additional $> 1\%$ of coastal tidal variability at scales below 4 km. This suggests future models need to maintain at least this resolution in order to remove such variability. Lastly, testing showed that combining independent tide models, here FES2022 and EOT20, yielded superior solutions to both models in isolation. As this is naturally accommodated in the GOAT framework, future work may look to produce hybrid products which utilize more global tide solutions, which has shown promise in recent mean-sea surface products Laloue et al. (2025).

A limitation of the present atlas is that it has only been released for latitudes between -66 and 66 degrees. This design decision was made to keep the products used to train GOAT-1C consistent, e.g. the full Jason-Sentinel-6 satellite coverage, which is a backbone orbit for tidal research. However, polar regions are a key area of tidal research and have some of the largest uncertainties in modern global tide models. As such, future extensions of GOAT-1C and applications of the GOAT framework to polar regions should be pursued using a combination of Cryosat, SWOT, and other historical missions with higher inclinations. Preliminary work in the Foxe Basin using SWOT Science Orbit data has shown promising results over conventional harmonic and response methods. However, consideration will need to be given to handling seasonal sea-ice and other geophysical corrections in these regions. An advantage of the present approach is the relative computational efficiency of the approach. Training the 20-model ensemble took <15 hours on a high-performance-computing cluster. As such, model iteration can be done quickly, potentially enabling more frequent updates of the atlas.

https://doi.org/10.5194/essd-2026-735
Preprint. Discussion started: 14 September 2026

7 Conclusions

The GOAT-1C atlas is a new global coastal tide model built on top of the FES2022 atlas and is the first to be trained on SWOT wide-swath altimetry. The model demonstrates consistent improvements relative to FES2022 across several independent measures, including gauges, conventional altimetry, wide-swath altimetry, and shoreline imaging. The largest gains are found in macrotidal and poorly resolved coastal regions. The new atlas provides uncertainty estimates that can be used to identify where and where not to use the product. The model can also be utilized as a post-hoc, observationally estimated FES2022 coastal uncertainty product, which provides a data-driven estimate of the magnitude of tidal variability FES2022 misses in a given region. The GOAT approach can be applied to any global tide model and trains in hours on the entire historical altimetry record, enabling rapid iteration. The priority with GOAT-1C is the coastal zone, largely a result of the downstream applications we plan to use GOAT-1C for. However, as the results from the GOAT framework are encouraging, an expansion not only into the polar regions but also into the open ocean would be a clear future avenue of research. While, the general consensus is that global models are converging in the open ocean (see (Ray, 2025) for a validation of state-of-the-art models in the open ocean), the expansion to the full global ocean would increase the usability of GOAT to a broader range of applications, including as model boundary forcings or for geodetic applications such as serving as corrections for satellite altimetry and gravimetry.

Data availability. The GOAT-1C atlas, including full documentation and example usage are provided: doi.org/10.5281/zenodo.22637903. During review this can be previewed at (Monahan and Hart-Davis, 2026). TICON-4 is available at: https://www.seanoe.org/data/00980/109129/.

https://doi.org/10.5194/essd-2026-735
Preprint. Discussion started: 14 September 2026

Appendix A: Additional Results

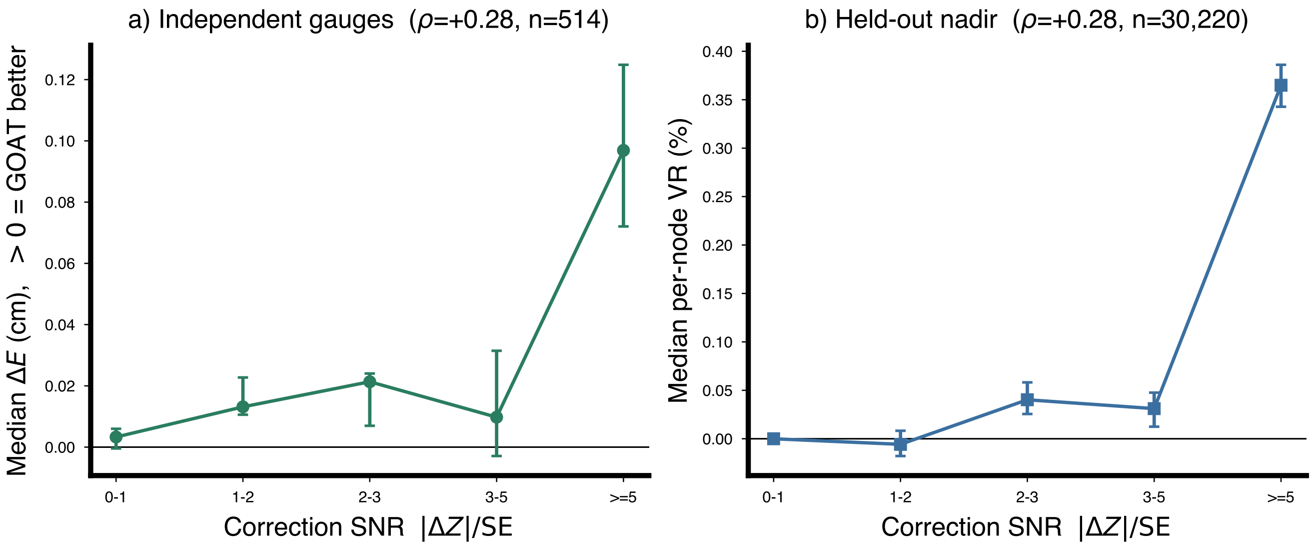

Figure A1. Realized skill rises with GOAT correction confidence. a) Independent TICON tide gauges: median per-gauge improvement $\Delta E = E_{\mathrm{FES2022}} - E_{\mathrm{GOAT}}$ (cm; > 0 means GOAT-1C is closer to the gauge) for M_2, binned by the ensemble correction signal-to-noise ratio $|\Delta Z|/\mathrm{SE}$. b), Held-out nadir altimetry: median per-node variance reduction (%) of the GOAT-1C correction over FES2022, binned by the same SNR (>0 means GOAT reduces variance). Markers are medians with bootstrap 95% confidence intervals; the nadir panel pools $\sim$2.4M held-out observations over 30,220 coastal nodes, versus 514 gauges in a). Both panels show near-parity with FES2022 at low SNR and a generally increasing skill gain at high SNR, with matching rank correlation (Spearman $\rho \approx +0.28$ on both).

https://doi.org/10.5194/essd-2026-735
Preprint. Discussion started: 14 September 2026

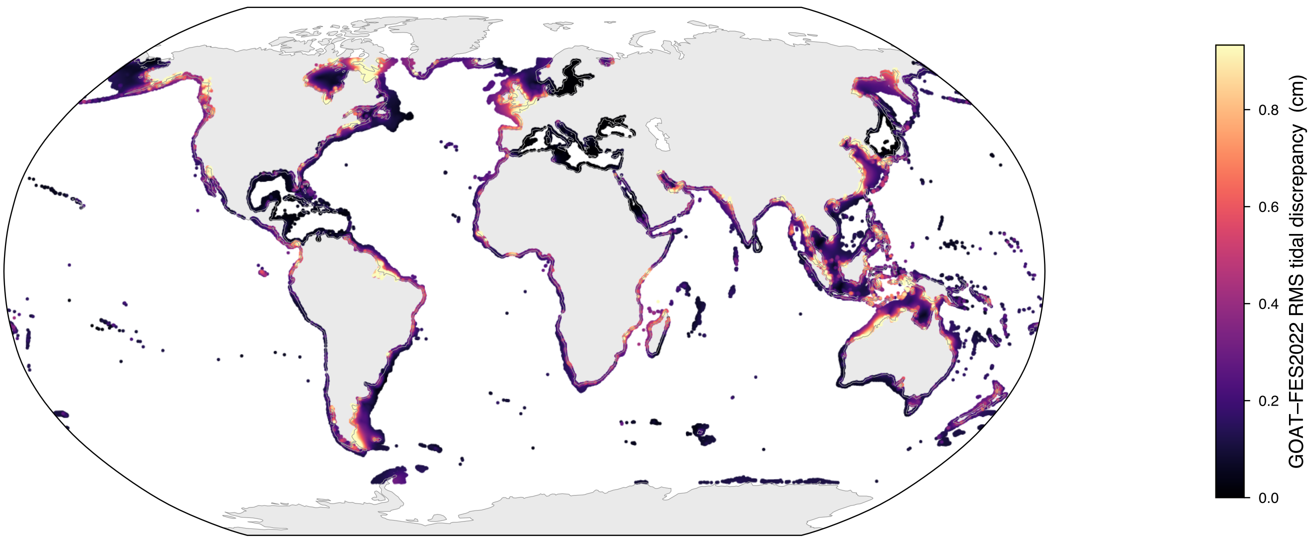

Figure A2. GOAT-1C as observationally-constrained discrepancy estimates for FES2022 at the coast. For each coastal node the model's per-constituent complex correction to FES2022, $dZ_k = Z_k^{\mathrm{GOAT}} - Z_k^{\mathrm{FES}}$, is collapsed into the time domain. The RMS tidal-elevation of FES2022 - GOAT-1C, $\sqrt{\frac{1}{2}\sum_k |dZ_k|^2}$ (cm) is then computed to produce a data-driven estimate of how far FES2022 departs from the altimetric observations at the coast in terms of resolvable tidal variability.

https://doi.org/10.5194/essd-2026-735
Preprint. Discussion started: 14 September 2026

Open Access Earth System Science Data Discussions

Table A1. TICON4 tide gauge validation across all constituents. Complex vector error, and amplitude/phase of FES2022 versus the GOAT product, per constituent (bold = better). Estimated over 514 gauges, with gauges assimilated into FES2022 removed. Constituents are ordered by global percentage statistically significant. Note all constituents are utilized, e.g. uncertainty gating is not employed.

	RMS (cm)		Median (cm)		Amplitude error (cm)		Phase lag error (deg)	
Constituent	FES2022	GOAT	FES2022	GOAT	FES2022	GOAT	FES2022	GOAT
M_2	21.40	**21.31**	2.71	**2.55**	**1.23**	1.26	3.4	**3.2**
K_1	5.76	**5.62**	0.83	**0.81**	0.40	**0.37**	**3.2**	3.4
S_2	**5.56**	5.57	1.14	**1.13**	**0.51**	0.59	4.9	**4.7**
N_2	4.34	**4.33**	0.70	**0.70**	**0.33**	0.33	4.3	**4.2**
M_4	2.88	**2.84**	0.45	**0.44**	0.23	**0.22**	**26.0**	27.1
P_1	1.50	**1.49**	0.38	**0.38**	0.23	**0.23**	**4.5**	4.6
O_1	**3.90**	3.91	0.70	**0.65**	0.37	**0.35**	3.0	**2.8**
MS_4	2.25	**2.16**	0.29	**0.28**	**0.14**	0.15	45.1	**43.8**
MN_4	1.19	**1.15**	0.25	**0.24**	0.11	**0.10**	47.1	**45.4**
K_2	1.74	**1.74**	0.45	**0.45**	**0.21**	0.23	**6.2**	6.5
M_f	**0.88**	0.88	**0.37**	0.38	**0.19**	0.23	16.4	**15.9**
M_6	1.71	**1.68**	0.24	**0.24**	**0.10**	0.10	60.1	**59.2**
M_3	**0.70**	0.70	0.29	**0.29**	**0.21**	0.21	98.5	**97.1**
MS_f	1.10	**1.07**	**0.49**	0.50	0.32	**0.31**	**51.7**	57.4
M_8	**0.60**	0.61	0.06	**0.06**	**0.02**	0.03	81.0	**80.9**
N_4	0.34	**0.34**	0.09	**0.08**	0.04	**0.04**	**55.1**	55.5
S_4	0.34	**0.33**	0.11	**0.11**	**0.06**	0.07	75.7	**71.9**
Q_1	**0.86**	0.87	**0.23**	0.24	**0.12**	0.13	**4.5**	4.7
μ_2	2.40	**2.40**	**0.42**	0.43	0.22	**0.21**	12.4	**12.1**
MM	1.23	**1.23**	0.67	**0.66**	**0.38**	0.41	35.3	**33.9**
ν_2	1.21	**1.20**	0.23	**0.23**	0.13	**0.13**	**6.2**	6.5
$^2N_2$	**0.64**	0.64	0.18	**0.18**	0.09	**0.09**	**7.7**	7.8
L_2	1.93	**1.93**	**0.31**	0.31	**0.17**	0.18	9.6	**9.6**
J_1	0.36	**0.34**	**0.14**	0.15	**0.07**	0.08	**9.9**	11.7
T_2	**1.08**	1.09	0.31	**0.29**	0.19	**0.18**	**15.4**	17.3
MKS_2	1.27	**1.27**	0.17	**0.17**	**0.11**	0.11	37.8	**36.7**
R_2	1.00	**1.00**	0.16	**0.16**	**0.08**	0.09	65.5	**64.7**
mean	2.53	**2.51**	0.46	**0.45**	**0.23**	0.24	29.3	**29.2**

https://doi.org/10.5194/essd-2026-735
Preprint. Discussion started: 14 September 2026

Open Access Earth System Science Data Discussions

Table A2. Realized GOAT skill versus ensemble correction SNR, on two independent datasets. $\rho_{\rm gauge}$ is Spearman's rank correlation between the correction SNR and the per-gauge improvement $\Delta E = E_{\rm FES2022} - E_{\rm GOAT}$ over the TICON4 gauges; $\rho_{\rm nadir}$ is the same against the per-node held-out-nadir variance reduction (VR). The remaining columns give the median per-node nadir VR (%) within each SNR bin ($n = 30{,}220$ nodes). Positive ρ means higher-confidence corrections realise more independent skill. Rows are constituents with at least 1,000 high-SNR (≥ 5) nadir nodes, plus the joint majors, sorted by $\rho_{\rm nadir}$. Median VR is used throughout (robust); p-values are omitted as they are anti-conservative under spatial non-independence.

			median nadir VR (%) by SNR bin				
Constituent	$\rho_{\rm gauge}$	$\rho_{\rm nadir}$	0-1	1-2	2-3	3-5	$\geq$5
M_2	+0.28	+0.28	+0.00	-0.01	+0.04	+0.03	+0.36
MS_4	+0.50	+0.16	+0.00	+0.02	+0.04	+0.07	+0.12
P_1	+0.06	+0.11	+0.00	+0.00	+0.01	+0.07	+0.05
MN_4	+0.43	+0.10	+0.00	+0.01	+0.01	+0.02	+0.04
S_2	+0.00	+0.07	+0.02	+0.07	+0.06	+0.14	+0.19
K_1	+0.13	+0.06	+0.00	+0.02	+0.01	+0.02	+0.08
N_2	+0.16	+0.04	+0.00	-0.00	-0.00	+0.01	+0.02
MS_F	+0.08	+0.03	+0.00	+0.02	+0.03	+0.01	+0.05
K_2	-0.04	+0.03	+0.00	+0.01	-0.00	+0.02	+0.06
M_6	+0.36	+0.02	+0.00	+0.00	+0.00	+0.00	+0.00
M_8	+0.20	-0.01	+0.00	-0.00	-0.00	+0.00	-0.01
M_4	+0.12	-0.02	-0.00	+0.00	-0.00	-0.01	-0.01
M_3	-0.11	-0.03	-0.00	-0.00	-0.00	-0.00	-0.01
O_1	+0.18	-0.06	+0.01	+0.01	+0.01	-0.07	-0.04
JOINT	–	+0.21	+0.08	+0.46	+0.45	+0.85	+1.78

https://doi.org/10.5194/essd-2026-735
Preprint. Discussion started: 14 September 2026

Appendix B: Dataset Production Details

B0.1 Atlas construction from the trained operator

The trained operator $g(\hat{\zeta})(\theta,\lambda,t)$ predicts sea level in the time domain; the released atlas expresses it as constituent-wise complex harmonic constants. For each of the coastal nodes we evaluate the operator over a synthetic reference year (2013) at hourly resolution. The FES2022 branch at the required lags is reconstructed from the node's FES2022 constants with the pyTMD equilibrium arguments (nodal corrections included) Sutterley et al. (2025), so the network sees exactly the input it saw in training; the dense coastal fine head is read at the nearest 4 km fine node and the training-only bias head is dropped. The resulting GOAT time series is analysed with UTide Codiga (2011) (ordinary least squares, no trend), yielding amplitude A_k and Greenwich phase lag g_k for the 31 resolvable constituents, and the complex constant $Z_k = (A_k/100)\,e^{-ig_k}$. Crucially, a pure-FES2022 series is passed through the *identical* UTide pipeline, and the correction is taken as the difference $\Delta Z_k = Z_k^{\mathrm{GOAT}} - Z_k^{\mathrm{FES}}$; this cancels any convention or nodal offset between UTide and the FES2022 grid. The corrected constant is $Z_k^{\mathrm{GOAT}} = Z_k^{\mathrm{FES}} + \Delta Z_k$. Each of the 20 ensemble members is analysed independently; the point estimate is the full-data member and the per-constituent standard error, SNR and FDR significance are formed from the spread of ΔZ_k across members. At EOT20-native nodes ΔZ_k is replaced by the learned FES+EOT20 blend on the shared constituents. Because the coastal nodes are the model's own evaluation nodes, no spatial interpolation of the constants is required.

Appendix C: Dataset Details and Usage

GOAT-1C is distributed as a single CF-style netCDF4 file, `goat1c_atlas_v1.nc`, with dimensions `(node=170698, constituent=31)`. The nodes are unstructured coastal points at ∼4 km spacing within $|\mathrm{lat}| \leq 66°$ (the nadir-altimetry coverage limit); this is *not* a regular latitude/longitude grid and does not load into gridded tide engines. Coordinates are `lon` (°E, $[-180, 180]$) and `lat` (°N). The constituent axis carries the lower-case constituent names.

Each node/constituent cell stores the GOAT-1C tide (`goat_amp` in cm, `goat_pha` in degrees), and the learned correction (`corr_amp`, `corr_pha`, = GOAT−FES2022). Complex constants follow $Z = (A/100)\,e^{ig}$ (metres), i.e. g is a Greenwich phase *lag*; phase should be interpolated only through the complex coefficients, never as an angle. The correction uncertainty is given by `se` (bootstrap standard error of $|\Delta Z|$, cm), `snr` (= $|\Delta Z|/\mathrm{SE}$) and `sig` (Boolean, significant at 5 % BH-FDR). These describe the DeepONet correction; at `eot20_blended` nodes the shipped constant is the FES+EOT20 blend while `se`/`snr`/`sig` still describe the DeepONet component (see Section 4.2.4).

Two per-node flags qualify each node: `eot20_blended` (True at the 29,206 EOT20-native nodes where the correction was refined by the learned FES+EOT20 blend; False = DeepONet only), and `valid` (False at 477 estuary/void nodes where FES2022 is undefined; there the amplitude/phase are NaN and `se`/`snr`/ `sig` are NaN/False). Users should mask on `valid` (equivalently `isfinite(goat_amp)`).

The recommended tidal product uses 28 constituents: the 31 in the file minus `s1`, `sa`, `ssa`, which mix non-tidal seasonal/radiational signal and default to FES2022 (they are excluded from the blend). Three FES2022 constituents that UTide

https://doi.org/10.5194/essd-2026-735
Preprint. Discussion started: 14 September 2026

Table B1. GOAT-1C model and training configuration.

Item	Value
Branch network	MLP, 3 layers, width 128, SiLU
Continuous (coarse) trunk	MLP(x, y, z), 3 layers, width 128, SiLU; no graph
Fine head	dense per-node free latent on a 4 km global coastal grid
	(1,485,184 nodes $\leq$ 30 km from coast)
Fine-head gate γ_j	$\sigma\big((15 - d_j)/5\big)$, $d_j =$ distance to coast (km)
Fine-head regularisation	graph-Laplacian smoothness $\lambda = 10^{-3}$; weight decay 0.03
Bias head	MLP$(x, y, z) \to 1$, SWOT-only, dropped at inference; $L_2 = 10^{-3}$
Latent dimension p	128
Activation	SiLU
Lag interval / number	$\{-24, -22, \ldots, 0\}$ h ($\tau = 2$ h) / 13
Batch composition	pooled nadir + SWOT; single loader
SWOT:nadir weighting	loss $= L_{\text{nadir}} + L_{\text{SWOT}}$, each count-normalised per source
Pixel weighting within SWOT	uniform ($\alpha = 0$)
Loss	bias-invariant Smooth-L_1 (Huber), $\beta = 0.10$
Optimizer	Adam, lr 3×10^{-4}, cosine schedule, 1000-step warmup
Weight decay	10^{-3} (base) / 0.03 (fine latent); grad-clip 1.0
Steps / batch size	40,000 / 8,192
Input/target normalisation	per-lag branch standardisation; target (total SL)
	standardised ($\mu = -0.001$ m, $\sigma = 0.513$ m)
Fine-grid spacing / assign radius	4 km / 6 km (1.5$\times$ cell)
Train/val/test split	random 5% val of science orbit; test = independent
	Cal/Val 1-day-repeat window; seed 42
Ensemble size	20
Bootstrap unit	SWOT pass (Poisson(1) block bootstrap); seed 0 = point est.
Random seed	42
Hardware	single NVIDIA V100 GPU
Training duration	$\approx$ 4 hours on HPC

cannot resolve — `lambda2`, `msqm`, `mtm` — are not in the atlas; take these directly from FES2022. More generally, for any constituent or location outside atlas coverage the correct fallback is FES2022 itself ($\Delta Z = 0$). "Free" (non-blended) nodes carrying no independent altimetry are the model's inductive spatial prediction; skill is validated at the observation nodes and against independent gauges and SWOT Cal/Val (the `snr` field self-documents extrapolation). Time-series reconstruction requires astronomical/nodal corrections; use the pyTMD equilibrium arguments with `corrections='FES'` so nodal handling matches FES2022. Global attributes record the constituent list, epoch year (2013), reference model, `lat_max`, `n_boot`

https://doi.org/10.5194/essd-2026-735
Preprint. Discussion started: 14 September 2026

Table C1. Variables in `goat1c_atlas_v1.nc`.

Variable	Dims	Units	Meaning / usage
`node`	node	–	integer node id (coord; stable across versions)
`constituent`	constituent	–	constituent name (coord), e.g. `m2`
`lon`, `lat`	node	°E, °N	node location, $\lvert\text{lat}\rvert \leq 66$
`eot20_blended`	node	bool	True: FES+EOT20 blend applied (29,206 nodes)
`valid`	node	bool	True where FES2022/GOAT defined; else amp/pha NaN
`goat_amp`, `goat_pha`	node×const	cm, deg	GOAT-1C tide (the product)
`corr_amp`, `corr_pha`	node×const	cm, deg	correction (GOAT − FES2022)
`se`	node×const	cm	bootstrap SE of the correction
`snr`	node×const	–	$\lvert\Delta Z\rvert/\text{SE}$
`sig`	node×const	bool	significant at 5 % BH-FDR

and `fdr_alpha`. A reference predictor (`goat_tide.py`, nearest-node/IDW + pyTMD) is provided. Note FES2022 is *not* included directly in the release, but can be downloaded on AVISO+ CNES (2024).

C0.1 Minimal Usage

1. **Locate the node.** Find the nearest coastal node to the target (λ, ϕ) (or inverse-distance-weight the few nearest); reject queries farther than ∼50 km. Keep only nodes with `valid=True`.
2. **Read the constants.** For each required constituent k take $Z_k^{\text{GOAT}} = (\texttt{goat\_amp}/100)\, e^{-i\,\texttt{goat\_pha}}$ (m).
3. **Apply the release/gated convention.** Use `goat_*` as delivered for the raw product; for the gated product, use `goat_*` where `sig=True` and fall back to `fes_*` where `sig=False` (equivalently add `corr_*` to FES2022 only where significant).
4. **Excluded/unresolved constituents.** Use FES2022 directly for `s1`, `sa`, `ssa` (recommended) and for the unresolved `lambda2`, `msqm`, `mtm` (not in the atlas). These values will need to be obtained from FES2022 and downloaded separately CNES (2024).
5. **Astronomical/nodal corrections.** Obtain (f_k, G_k) from `pyTMD.arguments`(MJD, constituents, corrections=‘FES’); this reproduces FES2022’s nodal handling for any epoch.
6. **Reconstruct.** $\eta(t) = \sum_k f_k\, A_k \cos\bigl(G_k(t) - g_k\bigr)$, with A_k, g_k from the chosen Z_k. Interpolate the complex Z_k (never the phase angle) if combining nodes.

https://doi.org/10.5194/essd-2026-735
Preprint. Discussion started: 14 September 2026

Table C2. Tidal constituents of the FES2022 atlas and their status in GOAT-1C. ✓: estimated and recommended in GOAT-1C ($n = 28$). †: provided by GOAT-1C but flagged unreliable in some regions, default to FES2022. –: not resolved by GOAT-1C.

Constituent	Description	GOAT-1C
Semidiurnal		
M_2	principal lunar	✓
S_2	principal solar	✓
N_2	larger lunar elliptic	✓
K_2	lunisolar declinational	✓
ν_2	larger lunar evectional	✓
μ_2	variational	✓
L_2	smaller lunar elliptic	✓
T_2	larger solar elliptic	✓
$2N_2$	lunar elliptic 2nd order	✓
ε_2	lunar	✓
R_2	smaller solar elliptic	✓
MKS_2	compound	✓
λ_2	smaller lunar evectional	–
Diurnal		
K_1	lunisolar declinational	✓
O_1	principal lunar	✓
P_1	principal solar	✓
Q_1	larger lunar elliptic	✓
J_1	smaller lunar elliptic	✓
S_1	solar (radiational)	†
Long-period		
Mf	lunar fortnightly	✓
Mm	lunar monthly	✓
MSf	lunisolar synodic fortnightly	✓
S_a	solar annual	†
S_{sa}	solar semiannual	†
$MSqm$	lunar	–
MTm	lunar	–
Shallow-water (overtides & compound)		
M_4	lunar quarter-diurnal	✓
MS_4	compound quarter-diurnal	✓
MN_4	compound quarter-diurnal	✓
N_4	quarter-diurnal	✓
S_4	solar quarter-diurnal	✓
M_3	lunar third-diurnal	✓
M_6	lunar sixth-diurnal	✓
M_8	lunar eighth-diurnal	✓

https://doi.org/10.5194/essd-2026-735
Preprint. Discussion started: 14 September 2026

Author contributions. TM conceptualized the study and methodology, managed project administration, and conducted the formal investigation including software development. MHD contributed to the investigation design and formal analysis interpretation, and data-processing. Both authors contributed various data as well as to writing (original draft, review, and editing).

Competing interests. The authors have no competing interests to declare.

Acknowledgements. TM acknowledges support from the Eric and Wendy Schmidt AI in Science Postdoctoral Fellowship, a Schmidt Futures program (No specific grant number). TM also acknowledges support from New College, University of Oxford.

https://doi.org/10.5194/essd-2026-735
Preprint. Discussion started: 14 September 2026

Open Access Earth System Science Data Discussions

References

Brown, J. M., Hibbert, A., Bricheno, L. M., Bradshaw, E., and Becker, A. E.: Chapter 11 - Tides at a coast, in: A Journey Through Tides, edited by Green, M. and Duarte, J. C., pp. 247–281, Elsevier, ISBN 978-0-323-90851-1, https://doi.org//10.1016/B978-0-323-90851-1.00019-4, 2023.

Carrere, L., Lyard, F., Cancet, M., Allain, D., Dabat, M.-L., Fouchet, E., Sahuc, E., Faugere, Y., Dibarboure, G., and Picot, N.: A new barotropic tide model for global ocean: FES2022, in: 2022 ocean surface topography science team meeting, p. 43, 2022.

Cartwright, D., Munk, W., and Zetler, B.: Pelagic tidal measurements: A suggested procedure for analysis, Eos, Transactions American Geophysical Union, 50, 472–477, 1969.

Cartwright, D. E.: A unified analysis of tides and surges round north and east Britain, Philosophical Transactions for the Royal Society of London. Series A, Mathematical and Physical Sciences, pp. 1–55, 1968.

Cartwright, D. E.: Tides: a scientific history, Cambridge University Press, 2000.

Cartwright, D. E. and Ray, R.: Oceanic tides from Geosat altimetry, Journal of Geophysical Research: Oceans, 95, 3069–3090, 1990.

Cazenave, A., Gouzenes, Y., Birol, F., Leger, F., Passaro, M., Calafat, F. M., Shaw, A., Nino, F., Legeais, J. F., Oelsmann, J., et al.: Sea level along the world's coastlines can be measured by a network of virtual altimetry stations, Communications earth & environment, 3, 117, 2022.

CNES: FES2022 (Finite Element Solution) Ocean Tide (Version 2022), [Data set], https://doi.org/10.24400/527896/A01-2024.004, funded by CNES, produced by LEGOS, NOVELTIS and CLS, distributed by AVISO, 2024.

Codiga, D. L.: Unified tidal analysis and prediction using the UTide Matlab functions, 2011.

Hart-Davis, M., Dettmering, D., and Seitz, F.: TICON-4: TIdal CONstants based on GESLA-4 sea-level records, PANGAEA https://www.seanoe. org/data/00980/109129, 2025.

Hart-Davis, M. G., Piccioni, G., Dettmering, D., Schwatke, C., Passaro, M., and Seitz, F.: EOT20: a global ocean tide model from multi-mission satellite altimetry, Earth System Science Data, 13, 3869–3884, https://doi.org/10.5194/essd-13-3869-2021, 2021.

Hart-Davis, M. G., Andersen, O. B., Ray, R. D., Zaron, E. D., Schwatke, C., Arildsen, R. L., Dettmering, D., and Nielsen, K.: Tides in Complex Coastal Regions: Early Case Studies From Wide-Swath SWOT Measurements, Geophysical Research Letters, 51, https://doi.org/10.1029/2024gl109983, 2024.

Hart-Davis, M. G., Monahan, T., Vos, K., and Andersen, O. B.: Beach scale tidal variations observed from satellite-derived shoreline time series, Communications Earth & Environment, 7, 680, 2026.

Laloue, A., Schaeffer, P., Pujol, M.-I., Veillard, P., Andersen, O., Sandwell, D., Delepoulle, A., Dibarboure, G., and Faugère, Y.: Merging recent mean sea surface into a 2023 Hybrid model (from Scripps, DTU, CLS, and CNES), Earth and Space Science, 12, e2024EA003 836, 2025.

Lu, L., Jin, P., Pang, G., Zhang, Z., and Karniadakis, G. E.: Learning nonlinear operators via DeepONet based on the universal approximation theorem of operators, Nature machine intelligence, 3, 218–229, 2021.

Moftakhari, H. R., AghaKouchak, A., Sanders, B. F., Feldman, D. L., Sweet, W., Matthew, R. A., and Luke, A.: Increased nuisance flooding along the coasts of the United States due to sea level rise: Past and future, Geophysical research letters, 42, 9846–9852, 2015.

Monahan, T. and Hart-Davis, M.: GOAT-1C Global Coastal Tide Atlas, https://zenodo.org/records/22637903?preview=1&token=eyJhbGci OiJIUzUxMiJ9.eyJpZCI6Ijg5Zjk3MjJiLTQzMGUtNDM3My04NDU5LWU4ODVlOThlMTU2MCIsImRhdGEiOnt9LCJyYW5kb20iO

https://doi.org/10.5194/essd-2026-735
Preprint. Discussion started: 14 September 2026

iIxYWVhYjRlNTJmNjliNzI0NjJmZTM5Zjg2OGJlM2M5MSJ9.c8W5-YaVzokDqj2m6ZfP3C8QdeLGDDMZNxzdAtBXIvS9x1LERE5TrwcDaYDWRLDz9sdl8XNJsuU3wKRtjPzSLg, 2026.

575 Monahan, T., Tang, T., Roberts, S., and Adcock, T. A.: RTide: Automating the tidal response method, Journal of Geophysical Research: Machine Learning and Computation, 2, e2024JH000 525, 2025a.

Monahan, T., Tang, T., Roberts, S., and Adcock, T. A.: Tidal corrections from and for SWOT using a spatially coherent variational Bayesian harmonic analysis, Journal of Geophysical Research: Oceans, 130, e2024JC021 533, 2025b.

Monahan, T. C., Polton, J., Innocenti, S., Matte, P., Ayyad, M., Saman, K., and Adcock, T. A.: Learning unresolved coastal dynamics in hydrodynamic models, 2026.

Munk, W. H. and Cartwright, D. E.: Tidal spectroscopy and prediction, Philosophical transactions for the Royal Society of London. Series A, mathematical and physical sciences, pp. 533–581, 1966.

Nilsson, B., Andersen, O. B., and Knudsen, P.: The DTU25 mean sea surface: from and for SWOT, Earth System Science Data, 18, 5027–5051, 2026.

585 Passaro, M., Cipollini, P., Vignudelli, S., Quartly, G. D., and Snaith, H. M.: ALES: A multi-mission adaptive subwaveform retracker for coastal and open ocean altimetry, Remote Sensing of Environment, 145, 173–189, https://doi.org//10.1016/j.rse.2014.02.008, 2014.

Ray, R. D.: Documentation for Goddard Ocean Tide solution GOT5: Global tides from multi-mission satellite altimetry, Tech. rep., National Aeronautics and Space Administration, 2025.

Schwatke, C., Dettmering, D., Passaro, M., Hart-Davis, M., Scherer, D., Müller, F. L., Bosch, W., and Seitz, F.: OpenADB: DGFI-TUM's Open Altimeter Database, Geoscience Data Journal, 11, 573–588, https://doi.org//10.1002/gdj3.233, 2024.

Stammer, D., Ray, R. D., Andersen, O. B., Arbic, B. K., Bosch, W., Carrere, L., Cheng, Y., Chinn, D. S., Dushaw, B. D., Egbert, G. D., et al.: Accuracy assessment of global barotropic ocean tide models, Reviews of geophysics, 52, 243–282, 2014.

Sutterley, T. C., Howard, S. L., Padman, L., and Siegfried, M. R.: pyTMD: Python-based tidal prediction software, Journal of Open Source Software, 10, 8566, 2025.

595 SWOT project: SWOT Level-2 KaRIn Low Rate SSH Expert (D), [Data set], https://doi.org/10.24400/527896/A01-2023.015, citation Expert L2_LR_SSH: "The SWOT L2_LR_SSH data product is produced and made freely available by the joint SWOT (NASA/JPL and CNES) project. L2_LR_SSH product quality is not final and will be affected by some evolutions as the SWOT project team makes progress on science data processing algorithms and instrument calibrations.", 2023.

Talke, S. A.: How tidal properties influence the future duration of coastal flooding, Npj Natural Hazards, 2, 36, 2025.

600 Turner, J., Iliffe, J., Ziebart, M., and Jones, C.: Global ocean tide models: assessment and use within a surface model of lowest astronomical tide, Marine Geodesy, 36, 123–137, 2013.

Vos, K., Splinter, K. D., Harley, M. D., Simmons, J. A., and Turner, I. L.: CoastSat: A Google Earth Engine-enabled Python toolkit to extract shorelines from publicly available satellite imagery, Environmental Modelling & Software, 122, 104 528, 2019.

Zetler, B. D. and Munk, W. H.: The optimum wiggliness of tidal admittances, 1975.